Chemistry Europe
European Chemical Societies Publishing

WILEY VCH

Excellence in Chemistry Research

Announcing our new flagship journal

- Gold Open Access
- Publishing charges waived
- Preprints welcome
- Edited by active scientists

Meet the Editors of *ChemistryEurope*

Luisa De Cola
Università degli Studi di Milano Statale, Italy

Ive Hermans
University of Wisconsin-Madison, USA

Ken Tanaka
Tokyo Institute of Technology, Japan

Chemistry–A European Journal
Research Article
doi.org/10.1002/chem.202300239
Chemistry Europe
European Chemical Societies Publishing
www.chemeurj.org

BODIPY-Perylene Charge Transfer Compounds; Sensitizers for Triplet-Triplet Annihilation Up-conversion

Ruben Arturo Arellano-Reyes,[a] Amrutha Prabhakaran,[a] Rengel Cane E. Sia,[b] Julien Guthmuller,[b] Keshav Kumar Jha,[c, e] Tingxiang Yang,[c, e] Benjamin Dietzek-Ivanšić,[c, e] Vickie McKee,[d] and Tia E. Keyes*[a]

Abstract: BODIPY heterochromophores, asymmetrically substituted with perylene and/or iodine at the 2 and 6 positions were prepared and investigated as sensitizers for triplet-triplet annihilation up conversion (TTA-UC). Single-crystal X-ray crystallographic analyses show that the torsion angle between BODIPY and perylene units lie between 73.54 and 74.51, though they are not orthogonal. Both compounds show intense, charge transfer absorption and emission profiles, confirmed by resonance Raman spectroscopy and consistent with DFT calculations. The emission quantum yield was solvent dependent but the emission profile remained characteristic of CT transition across all solvents explored. Both BODIPY derivatives were found to be effective sensitizers of TTA-UC with perylene annihilator in dioxane and DMSO. Intense anti-Stokes emission was observed, and visible by eye from these solvents. Conversely, no TTA-UC was observed from the other solvents explored, including from non-polar solvents such as toluene and hexane that yielded brightest fluorescence from the BODIPY derivatives. In dioxane, the power density plots obtained were strongly consistent with TTA-UC and the power density threshold, the I^{th} value (the photon flux at which 50% of ΦTTAUC is achieved), for B2PI was observed to be 2.5x lower than of B2P under optimal conditions, an effect ascribed to the combined influence of spin-orbit charge transfer intersystem crossing (SOCT-ISC) and heavy metal on the triplet state formation for B2PI.

Introduction

Photon up-conversion (UC) is a multiphoton photophysical process whereby photons of higher energy than those used to initiate photoexcitation are generated. Approaches to improving the efficiency of UC have implications across wide application spaces including cell imaging[1] sensing[2] photocatalysis[3] and solar energy harvesting[4]. One sub-type of up-conversion that is attracting increasing interest is triplet-triplet annihilation up-conversion (TTA-UC). TTA-UC typically has a low excitation threshold without the requirement for coherent visible and near-infrared (NIR) light sources, and this is a significant advantage over other types of up-conversion.[5,6]

In contrast to classical luminescence, where the emission is Stokes shifted, TTA-UC yields an anti-Stokes shifted emission via the process summarized in Scheme 1. In TTA-UC a sensitizer

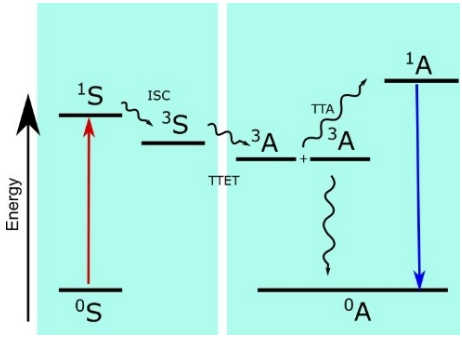

Scheme 1. Jablonski-Perrin diagram that illustrates the TTA-UC process. S = sensitizer A = Annihilator, ISC=Inter system crossing, TTET=Triplet- triplet energy transfer, TTA=Triplet- triplet annihilation. Only one sensitizer is shown in the scheme for clarity but two sensitizer molecules are required to produce two ^3A.

[a] R. A. Arellano-Reyes, A. Prabhakaran, Prof. T. E. Keyes
School of Chemical Sciences
National Centre for Sensor Research
Dublin City University
Glasnevin, Dublin 9 (Ireland)
E-mail: Tia.keyes@dcu.ie

[b] R. C. E. Sia, Dr. J. Guthmuller
Institute of Physics and Applied Computer Science
Faculty of Applied Physics and Mathematics
Gdańsk University of Technology
Narutowicza 11/12, 80233 Gdańsk (Poland)

[c] K. K. Jha, T. Yang, B. Dietzek-Ivanšić
Leibniz Institute of Photonic Technology Jena (IPHT)
Department Functional Interfaces
Albert-Einstein-Straße 9, 07745 Jena (Germany)

[d] Prof. V. McKee
Department of Physics, Chemistry and Pharmacy
University of Southern Denmark
Campusvej 55, 5230 Odense M (Denmark)

[e] K. K. Jha, T. Yang, B. Dietzek-Ivanšić
Institute of Physical Chemistry,
Friedrich Schiller University
elmholtzweg 4,, 07743 Jena (Germany)

Supporting information for this article is available on the WWW under https://doi.org/10.1002/chem.202300239

molecule (S) is excited to its first singlet state, by a long-wavelength photon. It then inter-system crosses to its first triplet state, ideally with high efficiency. The triplet sensitizer then undergoes (usually Dexter) energy transfer upon collision with the annihilator (A) (or emitter) leading to population of a triplet state of the annihilator. Two annihilators then, on mutual collision, undergo triplet-triplet annihilation leading to the population of a singlet state of one emitter partner and the ground state of the other. The species in the excited singlet then relaxes via fluorescence, yielding a photon of higher energy than that used to initiate the process.[7]

A good TTA-UC photosensitizer should have high molar absorptivity at visible or NIR wavelengths and high quantum efficiency of inter-system crossing. The sensitizer should also have a long-lived triplet excited state and, as shown in the Jablonski-Perrin diagram in Scheme 1, a critical thermodynamic criterion for efficient TTA-UC is that the energy of the sensitizer's first triplet state must exceed that of the energy of the emitters first triplet state.

Transition metal complexes have been widely studied in TTA-UC, as both sensitizers and annihilators.[8] They have found particular traction in this field because the heavy metal centre confers strong spin-orbit coupling, promoting formation of the essential triplet state of the sensitizer.[7,9] Furthermore, the Stokes shift between absorption and emission spectra in metal complex luminophores enables excitation without self-quenching at the relatively high concentrations required for TTA-UC to work. Effective as they are, there are drawbacks, metal complexes often have lower extinction coefficients than organic chromophores and transition metals such as ruthenium are expensive and rare.[9] Thus, there is rationale for seeking fully organic sensitizers for TTA-UC, but in the absence of a heavy metal centre, other approaches to promoting triplet yield must be found.

Boron-dipyrromethene (BODIPY) derivatives have emerged as effective organic alternatives to metal complex sensitizers in TTA-UC.[9–13] They offer numerous advantages including large extinction coefficients, and often robust photostability[5,14] but tend to exhibit poor intersystem crossing efficiency (ISC). Nonetheless, BODIPY has a versatile and well established synthetic chemistry that can be exploited to tune their photophysical properties[15] including implementing strategies to promote ISC. These strategies include promoting ISC rate through a) the El-Sayed rule, where originating and destination orbital type are different; b) through spin-orbit coupling via heavy-atom substitution;[16] for example, iodination or bromination; and c) through spin-orbit charge transfer intersystem crossing (SOCT-ISC). The latter can be accomplished by introducing donor-acceptor moieties onto the system whereby photoinduced electron transfer between the donor and acceptor subunits leads to the formation of a singlet charge-transfer state that undergoes charge recombination accompanied by a large change in orbital angular momentum that facilitates population of a triplet excited state (T_1).[17]

As BODIPY can behave as both excited state donor and acceptor there are numerous examples of BODIPY dyad and related structures that introduce charge transfer character into the optical properties of the derivative,[18–23] where donor or acceptor moieties are substituted at the pyrrole rings or the *meso* position at the methylylidene bridge. Indeed, this has been shown to lead to promotion of triplet quantum yield,[9,10,18,24] and the approach is drawing significant interest as a means of promoting singlet oxygen generation in BODIPY sensitizers for photodynamic therapy.[25,26] Though not as explored for TTA-UC applications it is proving an important approach to achieve metal free sensitization.[12,27–29] In addition, excitation into a charge transfer transition can lead to greater anti-Stokes shifts in resulting TTA-UC signal as well as environmental responsiveness. Perylene is a widely applied annihilator in TTA-UC systems and there have been several reports of dyad complexes that combine perylene with BODIPY where combination of dyad sensitizer and annihilator analogue lead to enhanced triplet yield and lifetime.[24,28,29] For example, Cui and co-workers[30] prepared a number of dyads, in which perylene was conjoined to a terminal ester by triazole link at the *meso* position. These species were effective sensitizers for TTA-UC with perylene as annihilator in solution. The same team reported a similar approach using a phenyl ring as the linker between the two fluorophores and the molecules thus produced were applied as annihilators with promising results. Indeed, they were found to be better annihilators than perylene, the benchmark triplet acceptor.[31] Wang and co-workers first reported the substitution of BODIPY with perylene at position 2 with promising results in photodynamic therapy.[24] Similar examples with anthracene have also been reported. In that case, the dyads were found to be highly efficient sensitizers, despite a strong solvent dependence. In this particular case, the formation of the long-lived triplet states observed were attributed to SOCT-ISC.[27]

In most reports to date, perylene has been appended to the *meso* or 8 position on the BODIPY core. This position is typically more electronically isolated[32] than substitution on the pyrrole rings and generation of charge transfer states, and rotational motion at this position, can lead to increased non-radiative decay of the electronically excited state.[18] Therefore, we were interested in understanding whether perylene at position 2/6 promotes TTA-UC sensitization through SOCT-ISC. With this in mind, we designed structures where methyl groups limit the co-planarity of the donor and acceptor, as orthogonality between this two units is necessary promote SOCT-ISC.[33–35] Furthermore, although the heavy atom effect and SOCT-ISC have been, separately, quite widely investigated as a means to promote triplet formation, there are relatively few studies examining the synergistic impact where both of these effects are combined. One reason this has not been widely investigated may be the challenges of unsymmetrically substituting BODIPY at the 2 and 6 positions. To this end, we describe herein a new synthetic route to BODIPY derivatives unsymmetrically substituted with perylene at the 2 position and H or I at the 6 position and report on the crystallography of the H- substituted compound. We compare the solvent dependent optical properties of iodinated and protonated compounds and evaluate their respective ability to sensitize TTA-UC.[36,37] We demonstrate both complexes show highly solvent-dependent TTA-UC where they

give a high intensity anti-Stokes output that is strongly promoted in the iodinated sensitizer. Supported by theoretical insights, we discuss the origin of this effect.

Results and Discussion

Synthesis of the dyads

With the purpose of obtaining efficient TTA-UC sensitizers, the asymmetric BODIPY derivatives, B2P and B2PI, shown in Scheme 2 were prepared according to Scheme 3. The first step

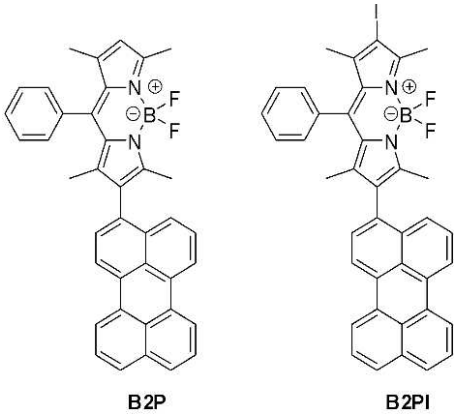

Scheme 2. Structures of the BODIPY-perylene heterochromophores studied in this work.

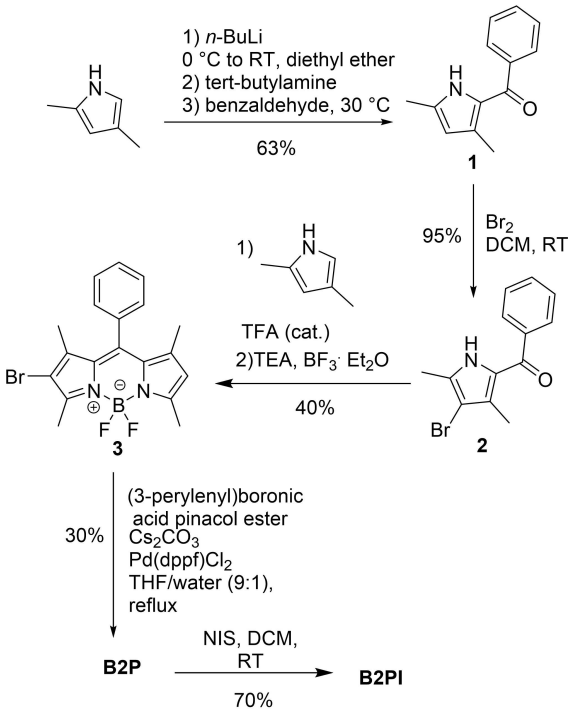

Scheme 3. Synthetic strategy to prepare B2P and B2PI.

was the synthesis of the ketopyrrole **1**, following a procedure modified from literature.[38]

We then carried out the halogenation of **1** using Br_2. Both steps were successfully optimized to avoid chromatography (isolation was by crystallization) and afforded the products in high purity and yield. The condensation of **2** with a second equivalent of 2,4-dimethylpyrrole and the complexation with BF_3 etherate through a one-pot, two-step procedure, afforded **3** in good yield. Taking this multistep synthetic approach meant we could avoid the use of *p*-chloranil, an oxidizing agent commonly used in the one-pot three steps synthesis of BODIPY, as it is not only difficult to handle and highly toxic but also did not produce a complete oxidation, from dipyrromethane to dipyrromethene, in multigram scale. B2P was prepared through the Suzuki-Miyaura coupling between intermediate **3** and (3-perylenyl)boronic acid pinacol ester (prepared in two steps, see Supporting Information, section 1). Despite efforts to optimise the reaction conditions, the yield was never greater than 30%. B2PI was then obtained by iodination of B2P with *N*-Iodosuccinimide (NIS).

Crystallography

The importance of orthogonality between the donor and acceptor moieties in SOCT-ISC has been widely discussed and crystallography can provide useful insights into the relative orientation of these moieties.[36,37] Dark red crystals of the chloroform solvate B2P·CH_3OH were obtained by vapour diffusion of methanol into a chloroform solution. The unsymmetric unit contains two independent but similar B2P conformers (referred to as molecules A and B) as well as some disordered methanol solvent. Figure 1 shows a perspective view of molecule A; molecule B has a similar conformation, but torsion of the perylene group renders it significantly less planar (Figure S14).The angles between the mean plane of the BODIPY core and the perylene group are 73.54(3)° and 74.51(4)° for molecules A and B, respectively. In this conformation, repulsive interactions between the BODIPY methyl groups (C22A and C25A) and the perylene system are reduced, however the two

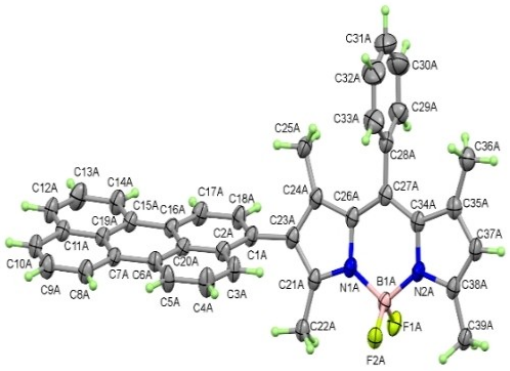

Figure 1. Perspective view of one of the two independent molecules of B2P (molecule A) showing 50% displacement ellipsoids.

fluorophores are not strictly orthogonal. Comparison with related structures in the Cambridge Structural Database[39] suggests this geometry is not unusual. Moreover, the DFT calculations, (Supporting Information) for the ground state geometry also point to non-orthogonal structures with angles of 59.5° and 59.7° for B2P and B2PI, respectively. Despite the very similar conformations, the intermolecular interactions differ markedly between the two independent molecules. Molecule A is paired with a symmetry equivalent molecule across a centre of inversion, leading to formation of π-stacked dimers (Figure S16), this stacking does not extend further through the structure and there is no equivalent stacking involving molecule B. Additionally, there are a number of (sp^2)C-H···F and (sp^2)C-H···π interactions linking the molecules in three dimensions (Figures S16 and S17).

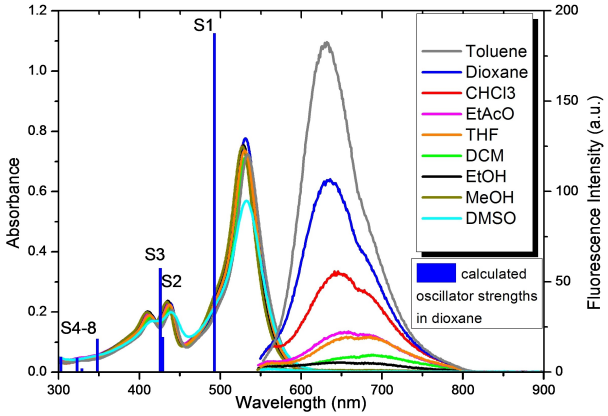

Figure 2. Absorption spectra of B2PI in different solvents at 10 μM, and emission data recorded with a 5 nm slit width. The calculated oscillator strengths for the S1 to S8 states are indicated in the vertical blue lines. The emission spectrum from cyclohexane is not shown as under the conditions used here it saturates the detection.

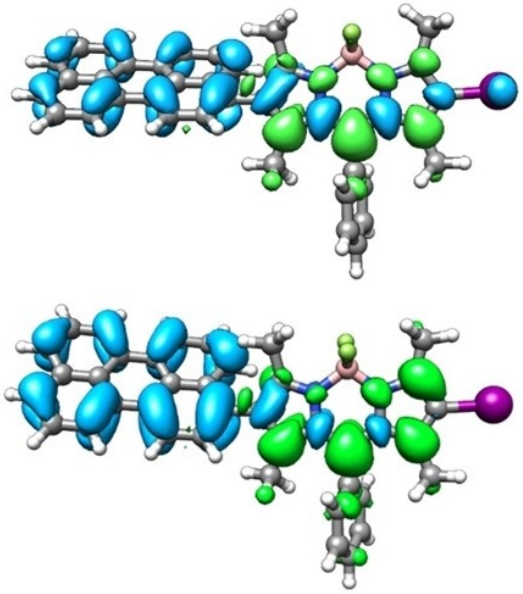

Figure 3. Isosurface of charge density difference for the S_1 excitation in B2PI. Positive (electron) and negative (hole) values are indicated in green and blue colours, respectively. (Top) at the S_0 geometry, (Bottom) at the S_1 geometry.

Absorption and emission properties

Figure 2 shows the absorption and emission spectra of B2PI across a range of solvents of different polarity. Also, indicated in vertical lines, are the computed oscillator strengths for each transition in dioxane. The absorption maxima occur at approximately 531 nm for B2PI and at 515 nm for B2P, and notably vary minimally with solvent in terms of spectral shape, position or intensity of the bands. Superficially, both absorptions, based on λ_{max} and extinction, appear characteristic of BODIPY localised $^1\pi$–π^* transitions consistent with the lack of solvent sensitivity. The absorbance is however, broader than expected for such a transition and TDDFT calculations as well as resonance Raman data, discussed below (see Figure 3) show that this (S_1) absorbance has significant perylene-to-BODIPY charge transfer character. Notably, although there is some variation with solvent, the extinction coefficients of B2P and B2PI exceeded 60,000, $M^{-1}\,cm^{-1}$) Both compounds also show well resolved absorption features between 400 and 430 nm, characteristic of perylene (Table S3). The emission spectra for both compounds are characteristic of a charge transfer excited state: Both the Stokes shift (around 3500 cm^{-1}) and the spectral width are much larger than expected for BODIPY emission. The CT character of emission is evident in all solvents explored.[21] The emission maxima shifts modestly to the red with increasing solvent polarity but the emission quantum yield is dramatically affected by solvent. The emission spectra shown in Figure 2 are absorbance matched at the excitation wavelength so the relative intensities directly reflect changes to the quantum yield with solvent. For reference, the absolute quantum yield for B2PI is 2.5% in dioxane (see Table 1).

Emission is most intense from non-polar solvents, (in cyclohexane the emission intensity saturated the detector under the conditions shown here) but is weak from polar and protic solvents including methanol and DMSO. Overall, irrespective of solvent the emission spectra of B2P and B2PI remain characteristic of CT states with no evidence of localised BODIPY centred emission from any of the solvents explored. This behaviour contrasts with reports of perylene derivatives, where perylene is substituted at the *meso* position.[28]

The charge transfer character of the S_1 state can be rationalised from DFT computation which shows that relaxation to the S_1 geometry of B2P/B2PI decreases the perylene-BODIPY rotation angle from 59.5/59.7° (S_0 geometry) to 41.7/41.7° (S_1 geometry). This partial planarization increases the extent of conjugation between the perylene and BODIPY fragments, to increase charge transfer character of S_1, Figure 3.[18,40] The calculated Stokes shifts, obtained from the vertical absorption and emission energies, for B2P and B2PI are 3606 and 3742 cm^{-1}, respectively (Table S7-S10). These values are in excellent agreement with experiment (around 3500 cm^{-1}).

To evaluate the impact of iodination on the photophysics of the compound, we compared the lifetime data for both

Table 1. Photophysical properties of B2P and B2PI in 1,4-Dioxane and toluene. SE = standard error. Mol. Bright. = molecular brightness.

Compound	Abs.λmax [nm], (ε [M^{-1} cm^{-1}])	Em. λ_{max}, [nm], φ_F [a]	DioxaneMol. Bright.	τ_1 [ns][b]	Amplitude [%]	τ_2 [ns][b]	Amplitude [%]	Average lifetime Intensity-weighted [ns]	k_r [c] [10^7 s^{-1}]	k_{nr} [c] [10^7 s^{-1}]
Dioxane										
B2P	515, (73291, SE = 0.013) 483[g]	625, 0.094[d] 585[g]	6889	4.1 ± 0.2	5.3	1.8 ± 0.01	94.7	2.0 ± 0.02	4.6 18[g]	44.4
B2PI	531, (67665 SE = 0.012) 493[g]	641, 0.025[e] 605[g]	1691	3.8 ± 0.1	94.6	0.6 ± 0.01	5.4	1.4 ± 0.01	1.8 15[g]	68.2
Toluene										
B2P	518, (80431 SE = 0.001)	616, 0.209	16810	2.5 ± 0.01	100	–	–	2.5 ± 0.01	8.5	32.1
B2PI	534, (63338 SE = 0.004)	636, 0.033	2090	2.9 ± 0.1	7.2	0.7 ± 0.01	92.8	1.2 ± 0.02	2.6	78.7

[a] Absolute quantum yields were obtained in an integrating sphere and have a ± 2% of error. [b] Lifetimes were recorded in triplicate (deaerated solutions in sup. Info Table S1). [c] Radiative decay rates calculated using $k_r = \Phi_F/\tau$. Non radiative decay estimated from $k_{nr} = (1\text{-}\Phi)/\tau$. [d] At 517 nm. [e] at 532 nm. [g] Theoretical values calculated with MN15/6-311 + + G(2d,p) level of theory.

compounds in dioxane and toluene, selected because emission is strong from both solvents but, as discussed below, TTA-UC is only observed from the former.

Table 1 shows that the absorbance and emission maxima of B2P are red shifted by about 20 nm on iodination in B2PI. While both compounds show similar extinction coefficients indicating that absorbance cross section is uninfluenced by iodination of the 6-position. This is confirmed from computation, which show nearly identical oscillator strengths of about 1.13 calculated for the S_1 excitation of B2P and B2PI (Table S6). Conversely, but as expected, the absolute fluorescence quantum yield is significantly reduced on iodination where Φ_F is 2.5% for B2PI excited at 532 nm in dioxane compared to 9.4% for B2P at the same excitation wavelength. The >6-fold difference in emission quantum yield can be ascribed to promotion of ISC by the heavy iodine atom.[41,42] Notably, both compounds show dual exponential fluorescence decays in dioxane. For B2P τ_1 was determined as 4.14 ns and τ_2 as 1.77 ns. As expected, iodination reduces the emission lifetime of both decay components but particularly of τ_2 which at 0.64 ns in B2PI, is at the limit of our instrument resolution. Deaeration of the solution has, within experimental error no effect on the lifetimes of the compounds. Interestingly, the lifetimes of B2P reverts to a single exponential decay in toluene, 2.51 ns. Again lifetime was independent of deaeration. The biexponential decay in dioxane is interesting and, the absence of oxygen dependence seems to indicate that a triplet state is not contributing. This may be due to different rotamers or some aggregation of the compound. However, we do not see evidence of this in concentration dependence studies, i.e. the relative amplitude of the dual components does not change with concentration.

Resonance Raman spectroscopy

To gain further insight into the origin of the lowest energy optical transition centred around 530 nm, we compared the resonance Raman (RR) spectra of B2P and B2PI under 474 nm excitation, which is pre-resonant with the λ_{max} and compared the data with the calculated RR spectrum (Figure 4, blue curve) to identify the resonantly enhanced features. (The complete band assignments are provided in the Supporting Information, Table S11.) There is excellent agreement between the measured and calculated RR spectra. The assignment of the bands (Table S11) shows that vibrational modes localized on both the BODIPY and perylene fragments are resonantly enhanced. This observation strongly indicates that both perylene and BODIPY contribute to the underlying absorption. This is further confirmed by calculating separately the RR spectra of the separate BODIPY and perylene moieties. Individually, as calculated, these spectra do not correspond to the experimental RR spectrum of B2PI (Figure S22 and S23).

In particular, the RR spectrum calculated for the BODIPY fragment (Figure S22), differs significantly from the measured B2PI RR spectrum. The data therefore indicate that for both B2P and B2PI (Figures 4 and S21) the initially populated S_1 state at the Franck-Condon geometry has significant charge transfer

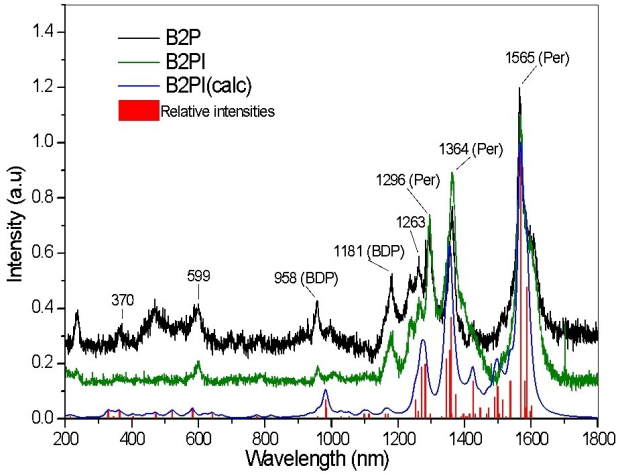

Figure 4. Resonance Raman spectra of B2P (black) and B2PI (green). Excitation at 473 nm in solid KBr. Computed resonance Raman spectrum of B2PI (blue). BDP = modes attributed to BODIPY Per = modes attributed to perylene.

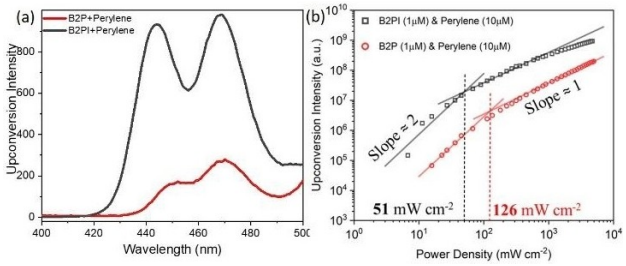

Figure 5. Up-converted emission from a) 5 μM B2P with 100 μM perylene, and 2.5 μM B2PI with 25 μM perylene in deaerated dioxane at 10 nm slit widths under 532 nm excitation, b) log (power density) vs log (up-conversion emission intensity at 443 nm) of B2P & B2PI with perylene in dioxane at 532 nm excitation.

character mixed with a BODIPY-centred excitation. The most intense features occur at 1565 cm^{-1} and an underlying shoulder around 1600 cm^{-1} both attributed to in plane C–C stretches of the perylene ring and in-plane stretches of the directly connected pyrrole ring on the BODIPY (Table S11). Other prominent Raman features are intense modes at 1364 cm^{-1} and 1296 cm^{-1} attributed to perylene in plane ring stretch modes coupled to BODIPY ring stretches and coupled to C–H bending modes on the methyl substituents. BODIPY centred modes appear at 958 cm^{-1}, 1181 cm^{-1} and as shoulders around 1425 cm^{-1} and 1530 cm^{-1}.

TTA-UC

Since effective ISC is a prerequisite of TTA-UC, we were interested to understand whether the formation of the triplet states through SOCT enabled TTA-UC in B2P and whether iodination in B2PI improved sensitizer performance. Throughout these studies, perylene was used as triplet annihilator due to its high fluorescence quantum yield and anticipated energy match to the triplet state of B2P and B2PI.

First, a range of ratios of sensitizer to annihilator was explored to optimise the TTA-UC output. TTA-UC intensity was found to be maximum at annihilator:sensitizer 1:20 (molar ratio) in the case of B2P and 1:10 for B2PI in deaerated dioxane. TTA-UC was evident under 532 nm laser irradiation as a structured anti-Stokes emission with maxima at 443 nm and 473 nm corresponding to the emission of perylene as shown in Figure 5a.[13,43]

Irradiating perylene alone with a 532 nm laser under identical conditions, no emission bands were observed between 420–490 nm in absence of sensitizer, confirming signal is due to up-conversion. In a second control, where conditions of TTA-UC were replicated but the solution was not deaerated, anti-Stokes emission was also absent. Thus both B2P and B2PI are effective up-conversion sensitizers.

Figure 5a compares the TTA-UC signal from the deaerated solution of perylene with B2P and B2PI respectively under optimised ratios and generated under identical conditions of excitation, so the data can be directly compared. From this figure it is evident that the TTA-UC output is >4-fold greater under B2PI sensitization. Power density dependences of the up-converted light were measured for both sensitizer/annihilator pairs. The excitation power density is plotted versus up-conversion intensity in Figure 6b. The strong and weak annihilation regimes are very clear for both systems, a feature that is a characteristic of the TTA-UC process. There is a sharp transition from low annihilation kinetic regime (slope of 2, where the decay of sensitized triplets rather than UC dominates the process) to the high annihilation regime (slope of 1, where annihilation reaches saturation) in each case. For B2PI, the threshold power density (I_{th} in Equation (1)) is reached at 51 mW cm^{-2} compared with 126 mW cm^{-2} for B2P. The I^{th} value for B2PI which is 2.5x lower than of B2P allows direct insight into the influence of iodination on the kinetics of the TTA-UC process in a SOCT compound. The lower I^{th} value for B2PI systems likely associated with the higher ISC yield (φ_{ISC}), the fluorescence quantum yield (φ_F) for B2PI is 2.5% and for B2P is

Figure 6. Digital photograph of up-converted emission from 5 μM B2PI and 50 μM perylene in deaerated dioxane at 532 nm (power density 1.27 Wcm^{-2}) excitation.

12.3%, lower φ_F for B2PI indicates higher φ_{ISC}, since $\varphi_F + \varphi_{ISC} = 1$, neglecting the non-radiative decay channel.

$$I^{th} = \frac{(K_T)^2}{\phi_{TTET}\ \phi_{ISC}\ \alpha\ K_{TTA}} \quad (1)$$

Where φ_{TTET} is the efficiency of energy transfer from triplet sensitizer to ground state annihilator, α is the absorption extinction coefficient of sensitizer at the excitation wavelength. The k_T is the decay rate of triplet annihilator and the k_{TTA} is the bimolecular triplet-triplet annihilation rate.

The power density data corresponds well with TTA-UC emission data since under optimised conditions the B2PI, the iodinated sensitizer, generates an emission greater than 3-fold more intense compared to B2P in the optically matched system. Indeed, for both sensitizers, the perylene emission is clearly visible to the naked eye, Figure 6. The higher up-conversion efficiency of B2PI even when the sensitizer is present in lower concentration than B2P (see Supporting Information) is attributed to the enhanced ISC from the heavy atom effect. The dramatic improvement in TTA-UC performance with the iodine present, may suggest that SOCT-ISC and heavy atom effect work synergistically to promote triplet state lifetime. It is also interesting to note also that the relative intensity of the vibronic progression of the perylene emission varies with the sensitizer.

Notably, the observation, or not, of TTA-UC depended strongly on solvent. B2P and B2PI along with perylene under the optimised concentration conditions above, were tested across a series of solvents of different dielectric constants and polarity; acetonitrile, dioxane, THF, cyclohexane, toluene, DMSO, 1-butanol, hexane, ethyl acetate, dioxane + water mixture (3 : 2), and dichloroethane. Across all of these solvents, TTA-UC was only observed from dioxane and DMSO. Of these, TTA-UC efficiency was highest from dioxane (see Supporting Information Figure S12), but it is interesting to note that TTA-UC was also observed from DMSO although neither compound emits appreciably from this solvent. Conversely, it is notable that the highest quantum yields for emission at 630 nm (in absence of perylene) were observed from cyclohexane and toluene, but TTA-UC does not occur for either sensitizer in these solvents.

Solvent dependence of up-conversion quantum yield has been reported previously in a BODIPY system comprising an iodo-BODIPY (2,6-diiodo-1,3,5,7-tetramethyl-8-phenyl-4,4-difluoroboradiazaindacene) and perylene annihilator by Zhang et al.[44] They similarly observed highest quantum efficiency from dioxane but in contrast, reported lowest yield from DMSO and good TTA-UC efficiency from non-polar solvents including hexane, heptane and toluene, from which we observe no TTA-UC at all.

In the case of the previous work, viscosity effects were attributed to the greater quantum yield of TTA-UC in dioxane compared to the other solvents. But in DMSO the unexpectedly weak TTA-UC was attributed to the solvents influence on the parameter $\Delta E_{TTA} = 2E(T_1)\text{-}E(S_1)$, (twice the triplet energy less the singlet energy) of the perylene annihilator, which was estimated to be larger than expected and thus detrimental to TTA-UC. However, in the present case, in contrast, we observe TTA-UC from dioxane and DMSO only. While viscosity may play a role, computation shows that the triplet CT (T_3) lies at approximately 2.4 eV, which is very close in energy to the S_1 state (within approximately 0.1 eV) for both derivatives at both the S_0 and S_1 geometries (Tables S6–10). So, ISC is likely to occur between the S_1 charge transfer state to T_3 charge transfer state. The BODIPY centred triplet and the perylene centred triplet (T_1 and T_2) are lower in energy (1.5-1.7 eV). These states can be populated by internal conversion from the T_3 charge transfer state. Therefore, TTET toward the lowest triplet of the annihilator (perylene) might happen either from T_3 or from the perylene centred triplet T_1. The efficiency of these processes is likely dictated by the solvent ; its influence on the lifetime of the T_3 CT state, on the energies of the states, and ΔE_{TTA}, thus, leading to the observed solvent dependence of the TTA-UC.

Conclusions

In conclusion, the synthesis of unsymmetrically substituted BODIPY perylene charge transfer compounds, B2P and B2PI is reported, in which perylene was substituted at the 2, with or without iodination at the 6 positions and the crystal structure of B2P defined. B2P and B2PI show solvent independent absorption attributed to charge transfer transition and modestly solvent dependent mega Stokes shifted emission attributed to relaxation from intramolecular charge transfer state between BODIPY and perylene states. The iodinated compound shows > 6-fold reduction in emission quantum yield compared to the B2P, attributed to efficient ISC due to the heavy atom effect. Consistent with triplet state formation, both compounds were efficient sensitizers in TTA-UC, and the impact of iodination was further reflected in the efficiency of the TTA-UC from power density plots the I^{th} where the value for B2PI is 2.5x lower than of B2P in dearated dioxane. Notably however, occurrence of TTA was strongly solvent-dependent. Intense TTA-UC, visible by eye, was observed with perylene annihilator, but only from DMSO and dioxane from across a diverse range of over 10 solvents explored. Computational studies indicate that ISC in both derivatives most likely occurs from S_1 charge transfer state to T_3 charge transfer state from where TTET to perylene annihilator occurs. The solvent dependence of the process is then attributed to either solvent modulation of the match between the energies of T_3 state of the sensitizer and T_1 of the annihilator to the influence of solvent or potentially to the influence of solvent on the lifetime of the T_3 state of the sensitizer.

Experimental Section

TTA-UC measurements: A Varian Cary Eclipse fluorescence spectrophotometer was used for TTA-UC measurements with an additional 532 nm excitation laser of 10 mW power with 1 mm beam diameter of 1.27 Wcm^{-2} power density purchased from Edmund optics. The TTA-UC measurements were recorded by blocking the excitation line in bioluminescence measurement mode. The solution measurements were carried out by deaerating the sample

by purging N_2 for 30 min in a quartz cuvette of 1 cm path length. The up-converted emission was recorded across the range 400 to 500 nm to avoid the interference from the the excitation source.

Threshold power density measurements: 1 cm Schlenk cuvettes were used to keep solutions under inert atmosphere.

The emission spectra were recorded using an FLS980 emission spectrophotometer (Edinburgh Instruments) with a 532 nm (CW532-100, Roithner LaserTechnik GmbH) laser diode. A combination of neutral density filters (OD = 1 and/or 2) was used to record emissions at higher excitation powers.

Synthesis of 1: Ketopyrrole **1** was prepared following a modified reported procedure.[38] In a 100 mL round bottom flask 2,4-dimethylpyrrole (2 mL, 19.42 mmol) was dissolved in 30 mL of diethyl ether at 0 °C in an ice/water bath, *n*-BuLi 2.5 M in hexanes was added dropwise (8.55 mL, 21.37 mmol, 1.1 equiv.) and the bath was removed. After 1 h, tert-butylamine was added (1.2 mL, 9.71 mmol, 0.5 equiv.), after 30 minutes, 2 equivalents of benzaldehyde were added (3.96 mL, 38.85 mmol) and the reaction was heated and stirred at 30 degrees overnight. The solvent was removed under vacuum and 50 mL of hexane were added to precipitate the product. All the solids were filtered under vacuum and wash with 100 mL of water to remove salts. The product was dried under vacuum overnight. The product thus obtained was very pure and was used as such in the next step. Yield 63%. ^{1}H NMR ($CDCl_3$, 600 MHz): δ (ppm) 9.23 (br, 1H), 7.64–7.61 (m, 2H), 7.51–7.48 (m, 1H), 7.46–7.42 (m, 2H), 5.89–5.84 (m, 1H), 2.29 (s, 3H), 1.92 (s, 3H). ^{13}C NMR ($CDCl_3$, 150 MHz): δ (ppm) 185.8, 140.2, 135.8, 131.0, 130.9, 128.4 (2 C), 128.3 (2 C), 127.9, 113.2, 14.1, 13.3. HR-MS (ESI-TOF) *m/z*: calculated for $C_{13}H_{14}NO$ 200.1070 found 200.1069

Synthesis of 2: 1 g of **1** (5.02 mmol) was dissolved in 20 mL of dichloromethane, Br_2 (0.26 mL, 5.12 mmol, 1.2 equiv.) was added dropwise and the reaction stirred at RT overnight. The reaction was quenched with water, and the product extracted with DCM (3 x 30 mL), the combined organic phases were dried under vacuum and the product recrystallized from ethanol. The product obtained was highly pure and was used as such in the next step. Yield 95%. ^{1}H NMR ($CDCl_3$, 600 MHz): δ (ppm) 9.79 (br, 1H), 7.65–7.61 (m, 2H), 7.55–7.51 (m, 1H), 7.48–7.43 (m, 2H), 2.31 (s, 3H), 1.91 (s, 3H). ^{13}C NMR ($CDCl_3$, 150 MHz): δ (ppm) 185.8, 139.5, 133.9, 131.6, 128.6, 128.51(2 C), 128.50(2 C), 126.9, 102.5, 13.4, 12.5. HR-MS (ESI-TOF) *m/z*: calculated for $C_{13}H_{13}BrNO$ 278.0175 found 278.0175.

Synthesis of 3: 850 mg of **2** (3.06 mmol) were dissolved in 5 mL of DCM, 0.35 mL of 2,4-dimethylpyrrole (0.35 mL, 3.36 mmol, 1.1 equiv.) and 5 drops of trifluoroacetic acid were added. The reaction was stirred at RT for 24 h. 2.56 mL of triethylamine (18.34 mmol, 6 equiv.) and 3.02 mL of BF_3 diethyletherate (24.45 mmol, 8 equiv.) were added and the reaction proceed at room temperature overnight. Volatiles were removed under vacuum and the crude product was purified by column chromatography (silica gel) using cyclohexane:EtAcO (9:1) as eluent to afford 560 mg of 3 as a dark red solid with 45% yield. Single crystals of **3** were prepared by slow diffusion of vapor and analysed by X-Ray diffraction (see Supporting Information). ^{1}H NMR ($CDCl_3$, 600 MHz): δ (ppm) 7.52–7.47 (m, 3H), 7.29–7.24 (m, 2H), 6.04 (s, 1H), 2.60 (s, 3H), 2.58 (s, 3H), 1.39 (s, 3H), 1.37 (s, 3H). ^{13}C NMR ($CDCl_3$, 150 MHz): δ (ppm) 158.1, 151.5, 145.2, 142.0, 138.9, 134.8, 132.2, 129.9, 129.39, 129.36, 128.0, 122.28, 122.27, 110.71, 110.69, 14.9, 14.6, 13.6, 13.5. HR-MS (ESI-TOF) *m/z*: calculated for $C_{19}H_{18}BBrF_2N_2Na$ 425.0612 found 425.0610.

Synthesis of B2P: In a 50 mL round-bottom flask 300 mg of **3** (0.47 mmol), 225.2 mg of 3-(perylenyl) boronic acid pinacol ester (0.56 mmol, 1.2 equiv.), 485 mg of cesium carbonate (1.49 mmol, 3 equiv.) and 18.15 mg of $Pd(dppf)Cl_2$ were refluxed for 16 h in 10 mL of a 9:1 THF/water solution. The reaction was cooled down to room temperature and filtered through a pad of celite using diethyl ether. The filtrate was dried with MgSO4 and the solvents were removed under vacuum. The product was purified by column chromatography (silica gel) using cyclohexane:EtAcO (90:10) to afford 85 mg of B2P, 30% yield. Single crystals of **4** were prepared by slow diffusion of vapor and analyzed by X-ray diffraction (see Supporting Information). ^{1}H NMR ($CDCl_3$, 600 MHz): δ (ppm) 8.22–8.16 (m, 4H) 7.68(d, 3 J = 8.06 Hz) 7.51–7.45 (m, 5H), 7.45-7.41(m, 2H) 7.40–7.36 (m, 1H), 7.35–7.33 (m, 1H), 7.26 (d, ^3J = 7.60 Hz), 6.04 (s, 1H), 2.61 (s, 3H), 2.42 (s, 3H), 1.41 (s, 3H), 1.19 (s, 3H). ^{13}C NMR ($CDCl_3$, 150 MHz): δ (ppm) 156.0, 154.8, 143.7, 142.0, 140.8, 135.2, 134.8, 134.1, 131.94, 131.86, 131.7, 131.34, 131.3, 131.2, 129.3, 129.1, 129.0, 128.7, 128.1, 128.05, 128.0, 126.9, 126.74, 126.73, 126.01, 121.6, 120.52, 120.5, 120.4, 119.9, 14.8, 14.6, 13.5, 13.0. HR-MS (APCI) *m/z*: calculated for $C_{39}H_{29}BF_2N_2$ 574.2392 found 574.240.

Synthesis of B2PI: 75 mg of B2P (0.13 mmol) were dissolved in 5 mL of DCM, 35.25 mg of NIS were added (0.156 mmol, 1.2 equiv.) and the reaction proceeded at room temperature for 2 h. After this time, traces of the starting material were still visible on TLC so 0.6 equivalents of NIS were added (17.62 mg, 0.078 mmol) and the reaction stirred at RT overnight. Solvents were removed under vacuum and the product was purified by column chromatography (silica gel) using cyclohexane:EtAcO (95:5) to afford 64 mg of B2PI. 70% yield. ^{1}H NMR (CD_2Cl_2, 600 MHz): δ (ppm) 8.26–8.17(m, 4H), 7.73–7.68 (m, 2H), 7.55–7.47 (m, 5H), 7.47–7.41(m, 2H), 7.41–7.37 (m, 1H), 7.37–7.34(m, 1H), 7.29 (d, ^3J = 7.63 Hz), 2.65 (s, 3H), 2.39 (s, 3H), 1.43 (s, 3H), 1.21 (s, 3H). ^{13}C NMR (CD_2Cl_2, 150 MHz): δ (ppm) 157.6, 155.0, 144.0, 143.1, 142.4, 135.2, 135.1, 134.2, 133.3, 132.1, 131.9, 131.6, 131.4, 131.2, 131.0, 129.8, 129.7, 129.3, 128.9, 128.4, 128.39, 128.35, 128.3, 127.3, 127.08, 127.07, 126.1, 120.9, 120.8, 120.7, 120.2, 84.7, 16.9, 16.1, 13.8, 13.3. HR-MS (APCI) *m/z*: calculated for $C_{39}H_{28}BF_2IN_2$ 700.1358 found 700.136.

Theoretical methods: The quantum chemical calculations were performed with the Gaussian 16 program.[45] Density functional theory (DFT) was employed to calculate the geometry and the harmonic vibrational frequencies of the ground state (S_0), while time-dependent DFT (TDDFT) was used to compute the singlet and triplet excited states properties (i.e. energy, transition dipole moment, geometry). The DFT and TDDFT calculations were done with the MN15[43] exchange-correlation functional in association with the 6–311++G(2d,p) basis set. This combination of functional and basis set proved to be adapted for a previously investigated BODIPY dye.[46] The effects of the solvent (1,4-Dioxane, $\varepsilon = 2.2099$) were taken into account by the polarizable continuum model (PCM).[47] The conventional linear response (LR) theory was used for the excited states properties. The vertical absorption energies, oscillator strengths and gradients – employed for the simulation of resonance Raman (RR) intensities – were calculated using the non-equilibrium procedure of solvation, whereas the equilibrium procedure of solvation was employed to calculate the excited states geometries, transition dipole moments and vertical emission energies.

The radiative rate k_r and associated radiative lifetime ($\tau_r = \frac{1}{k_r}$) were obtained from the Einstein A_{if} coefficient[46,48]

$$k_r = A_{if} = \frac{\omega_{if}^3}{3\varepsilon_0 \pi \hbar^3} |\vec{\mu}_{if}|^2 \quad (2)$$

Within the two-states approximation of Equation (2), the radiative lifetime was estimated using the vertical emission energy (i.e. $\hbar\omega_{if}$) and the electronic transition dipole moment at the S_1 geometry.

The RR intensities of B2PI were calculated with the so-called simplified Φ_e approximation[49,50] using a local program. The RR spectrum was calculated within the Franck-Condon approximation assuming an excitation wavelength of 474 nm. The contributions of the S_1, S_2 and S_3 states were included in the simulated RR spectrum. To correct for the lack of anharmonicity and the approximate treatment of electron correlation, the harmonic frequencies were scaled by a factor of 0.96.

The charge density difference (CDD) were computed with the Multiwfn program[51] in order to characterize the nature of the excited states.

Deposition Numbers 2157992 (for B2P·[CH_3OH]), 2157530 (for **2**) contain the supplementary crystallographic data for this paper. These data are provided free of charge by the joint Cambridge Crystallographic Data Centre and Fachinformationszentrum Karlsruhe Access Structures service.

Acknowledgements

We want to thank the European Union's Horizon 2020 research and innovation programme under the Marie Skłodowska Curie Actions grant agreement No. 813920 LogicLab ITN for the funding. The calculations were performed at the Wrocław Centre for Networking and Supercomputing (grant No. 384) and at the Academic Computer Centre TASK in Gdańsk. Open Access funding provided by IReL.

Conflict of Interest

The authors declare no conflict of interest.

Data Availability Statement

Data available in supplementary material or on request to authors.

Keywords: BODIPY · sensitizer · TTA-UC · up-conversion

[1] P. P. Nampi, A. Vakurov, L. E. Mackenzie, N. S. Scrutton, P. A. Millner, G. Jose, S. Saha, *J. Biophoton.* **2019**, *12*, e201800256.
[2] K. Presley, J. Hwang, S. Cheong, R. Tilley, J. Collins, M. Viapiano, J. Lannutti, *Mater. Sci. Eng. C* **2017**, *70*, 76–84.
[3] B. D. Ravetz, A. B. Pun, E. M. Churchill, D. N. Congreve, T. Rovis, L. M. Campos, *Nature* **2019**, *565*, 343–346.
[4] L. Frazer, J. K. Gallaher, T. W. Schmidt, *ACS Energy Lett.* **2017**, *2*, 1346–1354.
[5] D. Lin, J. Zhong, S. Ji, Z. Yuan, L. Xing, Q. He, H. Zhang, Y. Huo, *Dyes Pigm.* **2021**, *185*, 108912.
[6] K. K. Jha, A. Prabhakaran, C. S. Burke, M. Schulze, U. S. Schubert, T. E. Keyes, M. Jäger, B. D. Ivanšić, *J. Phys. Chem. C* **2022**, *126*, 4057–4066.
[7] X. Guo, Y. Liu, Q. Chen, D. Zhao, Y. Ma, *Adv. Opt. Mater.* **2018**, *6*, 1700981.
[8] Z. Xun, Y. Zeng, J. Chen, T. Yu, X. Zhang, G. Yang, Y. Li, *Chem. Eur. J.* **2016**, *22*, 8654–8662.
[9] J. Zhao, W. Wu, J. Sun, S. Guo, *Chem. Soc. Rev.* **2013**, *42*, 5323.
[10] K. Chen, Y. Dong, X. Zhao, M. Imran, G. Tang, J. Zhao, Q. Liu, *Front. Chem.* **2019**, *7*, 821.
[11] T. Jia, Q. Wang, M. Xu, W. Yuan, W. Feng, F. Li, *Chem. Commun.* **2021**, *57*, 1518–1521.
[12] N. Kiseleva, M. A. Filatov, J. C. Fischer, M. Kaiser, M. Jakoby, D. Busko, I. A. Howard, B. S. Richards, A. Turshatov, *Phys. Chem. Chem. Phys.* **2022**, *24*, 3568–3578.
[13] S. Dartar, M. Ucuncu, E. Karakus, Y. Hou, J. Zhao, M. Emrullahoglu, *Chem. Commun.* **2021**, *57*, 6039–6042.
[14] B. Hinkeldey, A. Schmitt, G. Jung, *ChemPhysChem* **2008**, *9*, 2019–2027.
[15] R. G. Clarke, M. J. Hall, in *Adv. Heterocycl. Chem.* Elsevier, **2019**, pp. 181–261.
[16] M. A. El-Sayed, *J. Chem. Phys.* **1963**, *38*, 2834–2838.
[17] M. Lv, Y. Yu, M. E. Sandoval-Salinas, J. Xu, Z. Lei, D. Casanova, Y. Yang, J. Chen, *Angew. Chem. Int. Ed.* **2020**, *59*, 22179–22184; *Angew. Chem.* **2020**, *132*, 22363–22368.
[18] R. Hu, E. Lager, A. Aguilar-Aguilar, J. Liu, J. W. Y. Lam, H. H. Y. Sung, I. D. Williams, Y. Zhong, K. S. Wong, E. Peña-Cabrera, B. Z. Tang, *J. Phys. Chem. C* **2009**, *113*, 15845–15853.
[19] B. Carlotti, M. Poddar, F. Elisei, A. Spalletti, R. Misra, *J. Phys. Chem. C* **2019**, *123*, 24362–24374.
[20] J. S. Rocha-Ortiz, A. Insuasty, B. Insuasty, A. Ortiz, *J. Mol. Struct.* **2020**, *1206*, 127774.
[21] J. Strahan, B. C. Popere, P. Khomein, C. A. Pointer, S. M. Martin, A. N. Oldacre, S. Thayumanavan, E. R. Young, *Dalton Trans.* **2019**, *48*, 8488–8501.
[22] Z. Zhang, R. M. Edkins, J. Nitsch, K. Fucke, A. Steffen, L. E. Longobardi, D. W. Stephan, C. Lambert, T. B. Marder, *Chem. Sci.* **2015**, *6*, 308–321.
[23] D. T. Chase, B. S. Young, M. M. Haley, *J. Org. Chem.* **2011**, *76*, 4043–4051.
[24] Z. Wang, M. Ivanov, Y. Gao, L. Bussotti, P. Foggi, H. Zhang, N. Russo, B. Dick, J. Zhao, M. Di Donato, G. Mazzone, L. Luo, M. Fedin, *Chem. Eur. J.* **2020**, *26*, 1091–1102.
[25] L. Wang, Y. Qian, *Dyes Pigm.* **2021**, *195*, 109711.
[26] E. Bassan, A. Gualandi, P. G. Cozzi, P. Ceroni, *Chem. Sci.* **2021**, *12*, 6607–6628.
[27] Y. Lei, K. Chen, G. Tang, J. Zhao, G. G. Gurzadyan, *J. Photochem. Photobiol. Chem.* **2020**, *398*, 112573.
[28] M. A. Filatov, S. Karuthedath, P. M. Polestshuk, S. Callaghan, K. J. Flanagan, T. Wiesner, F. Laquai, M. O. Senge, *ChemPhotoChem* **2018**, *2*, 606–615.
[29] Z. Wang, J. Zhao, M. Di Donato, G. Mazzone, *Chem. Commun.* **2019**, *55*, 1510–1513.
[30] X. Cui, A. M. El-Zohry, Z. Wang, J. Zhao, O. F. Mohammed, *J. Phys. Chem. C* **2017**, *121*, 16182–16192.
[31] X. Cui, A. Charaf-Eddin, J. Wang, B. Le Guennic, J. Zhao, D. Jacquemin, *J. Org. Chem.* **2014**, *79*, 2038–2048.
[32] S. Kim, J. Bouffard, Y. Kim, *Chem. Eur. J.* **2015**, *21*, 17459–17465.
[33] Y. E. Kandrashkin, Z. Wang, A. A. Sukhanov, Y. Hou, X. Zhang, Y. Liu, V. K. Voronkova, J. Zhao, *J. Phys. Chem. Lett.* **2019**, *10*, 4157–4163.
[34] Z. E. X. Dance, S. M. Mickley, T. M. Wilson, A. B. Ricks, A. M. Scott, M. A. Ratner, M. R. Wasielewski, *J. Phys. Chem. A* **2008**, *112*, 4194–4201.
[35] T. Okada, I. Karaki, E. Matsuzawa, N. Mataga, Y. Sakata, S. Misumi, *J. Phys. Chem.* **1981**, *85*, 3957–3960.
[36] H. Klfout, A. Stewart, M. Elkhalifa, H. He, *ACS Appl. Mater. Interfaces* **2017**, *9*, 39873–39889.
[37] A. Martin, R. D. Moriarty, C. Long, R. J. Forster, T. E. Keyes, *Asian J. Org. Chem.* **2013**, *2*, 763–778.
[38] Z. Guo, X. Wei, Y. Hua, J. Chao, D. Liu, *Tetrahedron Lett.* **2015**, *56*, 3919–3922.
[39] C. R. Groom, I. J. Bruno, M. P. Lightfoot, S. C. Ward, *Acta Crystallogr. Sect. B* **2016**, *72*, 171–179.
[40] J. Moon Lee, S. Bum Yuk, J. Woong Namgoong, J. Pil Kim, *Dyes Pigm.* **2021**, *185*, 108864.
[41] B. C. De Simone, G. Mazzone, J. Pirillo, N. Russo, E. Sicilia, *Phys. Chem. Chem. Phys.* **2017**, *19*, 2530–2536.
[42] E. Bassan, Y. Dai, D. Fazzi, A. Gualandi, P. G. Cozzi, F. Negri, P. Ceroni, *Photochem. Photobiol. Sci.* **2022**, *21*, 777–786.
[43] K. Chen, W. Yang, Z. Wang, A. Iagatti, L. Bussotti, P. Foggi, W. Ji, J. Zhao, M. Di Donato, *J. Phys. Chem. A* **2017**, *121*, 7550–7564.
[44] Q. Zhou, M. Zhou, Y. Wei, X. Zhou, S. Liu, S. Zhang, B. Zhang, *Phys. Chem. Chem. Phys.* **2017**, *19*, 1516–1525.
[45] M. J. Frisch, G. W. Trucks, H. B. Schlegel, G. E. Scuseria, M. A. Robb, J. R. Cheeseman, G. Scalmani, V. Barone, G. A. Petersson, H. Nakatsuji, X. Li, M. Caricato, A. B. Marenich, J. Bloino, B. G. Janesko, R. Gomperts, B. Mennucci, H. P. Hratchian, J. V. Ortiz, A. F. Izmaylov, J. L. Sonnenberg, D. Williams-Young, F. Ding, F. Lipparini, F. Egidi, J. Goings, B. Peng, A. Petrone, T. Henderson, D. Ranasinghe, V. G. Zakrzewski, J. Gao, N. Rega, G. Zheng, W. Liang, M. Hada, M. Ehara, K. Toyota, R. Fukuda, J. Hasegawa, M. Ishida, T. Nakajima, Y. Honda, O. Kitao, H. Nakai, T. Vreven,

K. Throssell, J. A. Montgomery Jr., J. E. Peralta, F. Ogliaro, M. J. Bearpark, J. J. Heyd, E. N. Brothers, K. N. Kudin, V. N. Staroverov, T. A. . Keith, R. Kobayashi, J. Normand, Raghavachari, A. P. Rendell, J. C. Burant, S. S. Iyengar, J. Tomasi, M. Cossi, J. M. Millam, M. Klene, C. Adamo, R. Cammi, J. W. Ochterski, R. L. Martin, K. Morokuma, O. Farkas, J. B. Foresman, D. J. Fox, *Gaussian 16*, Gaussian, Inc., Wallingford CT, **2016**.
[46] R. C. E. Sia, R. A. Arellano-Reyes, T. E. Keyes, J. Guthmuller, *Phys. Chem. Chem. Phys.* **2021**, *23*, 26324–26335.
[47] J. Tomasi, B. Mennucci, R. Cammi, *Chem. Rev*. **2005**, *105*, 2999–3094.
[48] D. P. Craig, *Molecular Quantum Electrodynamics.* Dover Publications, **2012**.
[49] J. Guthmuller, *J. Chem. Phys.* **2016**, *144*, 064106.
[50] J. Guthmuller, in *Mol. Spectrosc. Quantum Chem. Approach Eds Ozaki M J Wójcik J Popp*, Wiley-VCH, **2019**, pp. 497–536.
[51] T. Lu, F. Chen, *J. Comput. Chem.* **2012**, *33*, 580–592.

Manuscript received: January 23, 2023
Accepted manuscript online: February 21, 2023
Version of record online: March 29, 2023